MIMO Transmission for Single-fed ESPAR with Quantized Loads

Ang Li, *Student Member, IEEE*, Christos Masouros, *Senior Member, IEEE*, and Constantinos B. Papadias, *Fellow, IEEE*

***Abstract*—Compact parasitic arrays in the form of electronically steerable parasitic antenna radiators (ESPARs) have emerged as a new antenna structure that achieves multiple-input-multiple-output (MIMO) transmission with a single RF chain. In this paper, we study the application of precoding on practical ESPARs, where the antennas are equipped with load impedances of quantized values. We analytically study the impact of the quantization on the system performance, where it is shown that while ideal ESPARs with ideal loads can achieve a similar performance to conventional MIMO, the performance of ESPARs will be degraded when only loads with quantized values are available. We further extend the performance analysis to imperfect channel state information (CSI). In order to alleviate the performance loss, we propose to approximate the ideal current vector by optimization, where a closed-form solution is further obtained. This enables the use of ESPARs in practice with quantized loads. Simulation results validate our analysis and show that a significant performance gain can be achieved with the proposed scheme over ESPARs with quantized loads. Finally, the tradeoff between performance and power consumption is shown to be favorable for the proposed ESPAR approaches compared to conventional MIMO, as evidenced by our energy efficiency results.**

***Index Terms*—MIMO, ESPARs, precoding, quantized loads, imperfect CSI, optimization.**

I. Introduction

MULTIPLE-INPUT-MULTIPLE-OUPUT (MIMO) systems have been widely acknowledged as a promising technology and simple forms of precoding schemes have already appeared in the communication standards [1][2]. Precoding techniques can transfer the computational burden from the user side to the base station (BS) side, and therefore for multiuser MIMO communications, precoding techniques have been widely studied for power and cost efficient UE devices [3]-[10]. Among precoding techniques, capacity achieving non-linear dirty paper coding (DPC) has been proposed to pre-subtract interference prior to transmission [3]. However, the DPC methods developed so far are generally impractical due to the complexity and the infinite length assumption of codewords for the encoding of the data. To retain the performance benefits of DPC, a number of non-linear precoding techniques such as vector perturbation (VP) and Tomlinson-Harashima precoding (THP) that can asymptotically achieve the channel sum capacity have been proposed in [4]-[8]. Despite the rate benefits these schemes offer, non-linear methods developed so far are still complex and impractical due to the adoption of the sophisticated sphere-search algorithms. Therefore, linear precoding techniques based on channel inversion (CI) in [11] that offer a much lower computational complexity have received increasing research attention recently. Compared to non-linear schemes, the performance of CI precoding is far from optimum. A regularized channel inversion (RCI) precoding is then proposed in [12] to provide performance and capacity gains over CI precoding. A correlation rotation (CR) linear precoding scheme is further proposed in [13] which offers additional performance gains by exploiting the constructive interference.

Existing studies on precoding techniques assume conventional antenna arrays at the transceivers with multiple radio-frequency (RF) chains, each connected to a different antenna element. However, the significant hardware burden imposed by the multiple RF chains and the consequent power consumption can be a limitation. Furthermore, the spacing between adjacent antennas for conventional MIMO is usually designed larger than half of the wavelength to avoid the spatial correlation and mutual coupling effect between antenna elements, which is also a limitation in practice. This is especially true for lightweight and small battery-powered devices with strict size constraints such as mobiles and small access points (APs), where the correlation effect and mutual coupling effect cannot be neglected. Towards this direction, an alternative single-fed compact antenna array, also known as ESPAR was proposed in [14] and emerged as a research focus recently [15]-[19]. Different from conventional MIMO where each antenna element is connected to a dedicated RF chain fed by an independent voltage source, in ESPAR the voltage is only fed at the sole active antenna element and the currents at all adjacent parasitic antennas are induced by the mutual coupling effects between ESPAR antennas, enabling the parasitic antennas to radiate. For the compact ESPARs, only one RF chain is needed and the small size constraint turns to be an advantage as the mutual coupling is exploited to form the desired signals. Furthermore, the mutual coupling and consequently the currents at each parasitic antenna port can be controlled by the tunable loads

Manuscript received October 4, 2016; revised January 27, 2017 and accepted April 4, 2017. The associate editor coordinating the review of this paper and approving it for publication was Prof. Tony Q.S. Quek. ($Corresponding\ author: Ang\ Li$)

A. Li and C. Masouros are with the Dept. of Electronic and Electrical Eng., University College London, Torrington Place, London, WC1E 7JE, UK (email: ang.li.14@ucl.ac.uk, chris.masouros@ieee.org). C. B. Papadias is with the Broadband Wireless and Sensor Networks Group, Athens Information Technology, 19002 Athens, Greece (email: papadias@ait.edu.gr)

This work was supported by the Royal Academy of Engineering, UK, the Engineering and Physical Sciences Research Council (EPSRC) project EP/M014150/1, and the China Scholarship Council (CSC).

This paper has been presented in part at IEEE ICC, Kuala Lumpur, Malaysia, 2016.

at each parasitic antenna element, such that ESPARs can form different radiation patterns. With ESPARs, the hardware complexity and power consumption can be well alleviated as we only need one RF chain and one power amplifier, which makes them a space- and energy-efficient alternative to conventional antenna array architectures. In practice a single-fed active element can support an antenna array with only a few parasitic elements, and therefore ESPARs are most promising for small-scale MIMO systems, such as femtocells, the remote radio heads (RRHs) for the future cloud radio access networks (C-RANs) and picocells. Therefore in this paper we focus our study on the small-scale single-fed ESPARs, and the extension to a large scale MIMO system can be realized by employing the multiple-active-multiple-passive (MAMP) antenna arrays [Chapter 8, 20].

Due to the benefits of ESPARs introduced above, ESPARs have received research attention recently as a promising candidate for the future communication systems. In [21]-[23], ESPAR is proposed for single-RF MIMO systems where spatial multiplexing is considered. Specifically, in [23], a loading scheme is proposed to support the multiplexing of two 16-QAM signals for ESPAR and the effect of impedance errors on the performance of ESPAR systems is also simulated. Nevertheless, the effect of the impedance errors on the system performance is not mathematically analyzed. In [24], precoding for ESPAR is discussed and a design guideline is introduced, where the feeding voltage for the central antenna element and the calculation of each tunable load is given. However, specific precoding scheme analysis is not included. An important result is reported in [25], where a new signal model is introduced for ESPARs and it is shown that the currents at the ports of the transmitting array can be considered as the input to the system. In [26], MIMO transmission with ESPARs is studied, where the convex optimization approach is employed to obtain the load values that satisfy the input impedance constraint for the ESPAR array. In [27], an extension of ESPARs is introduced, where a load modulated antenna array is proposed, and its application to massive MIMO is discussed. In [28], we consider Gaussian random impedance errors for ESPAR based MIMO systems, and the error effect on the system performance is shown. The combination of ESPARs with orthogonal frequency division multiplexing (OFDM) can be found in [29][30], where the channel estimation techniques and receiver structures are proposed respectively.

The above existing studies on ESPARs assume that each parasitic load has a continuous value range and can be tuned to any arbitrary values based on the desired radiation pattern. This may not be feasible in practice since the electronic components implementing the load impedances (varactors, phase shifters, etc) may only take values with finite precision. This is critical for the application of ESPAR based MIMO, as the radiation pattern is controlled by tuning the load impedances of the passive antennas. Therefore, instead of considering the additive Gaussian random errors for the load impedances in [28], in this paper we focus on the more realistic ESPAR based MIMO systems with quantized load impedances and consider precoding schemes at the transmitter side. Closed-form expressions for the exact computation of the tunable loads and the feeding voltage are firstly given. For ESPAR-based MIMO, in realistic scenarios where there exist i) load impedance errors due to the quantized load values and ii) imperfect channel state information (CSI) due to channel estimation errors, the system performance might be degraded. We therefore provide a performance analysis of ESPARs with quantized loads. This effect is particular for ESPAR-based MIMO systems and has not been well investigated yet. To be specific, as the antenna spacing for ESPARs is small, we firstly characterize the semi-correlated channel model and the corresponding imperfect CSI model. Then, we study the impact of the mismatch effect introduced by the quantized loads and imperfect CSI on the system performance, and analytically derive the received signal-to-noise-ratio (SNR) and probability of error for CI precoding in the presence of these two effects. It will be shown that the impedance errors introduced by the quantized loads can be regarded as an additional noise term that is independent of the transmit SNR, which results in an error floor observed at high SNR regime. Noting the performance degradation introduced by the quantized loads, we then propose to approximate the current vector of the ESPAR array to the desired signal vector by convex optimization to compensate for the performance degradation. We propose to jointly optimize the feeding voltage and the quantized loads, where it is further proven that any additional variations in the quantized loads can only lead to an additional performance loss. Therefore, the resulting optimization problem is reduced to an optimization on the feeding voltage only, where we keep the values of the quantized loads unchanged. A closed-form solution of the optimal feeding voltage is further obtained, and the proposed scheme can be efficiently applied, without incurring significantly additional complexity. Numerical results show that the proposed scheme can compensate for the performance loss introduced by the quantized loads and better approach the performance of conventional MIMO systems, which enables the application of ESPARs with quantized loads in practice. It is also shown that the energy efficiency is more favourable for ESPARs even with quantized loads, due to the limited RF hardware complexity.

For reasons of clarity we summarize the contributions of the paper as:

1) We introduce the practical ESPAR based MIMO systems with quantized load impedances, where the linear precoding structure is introduced and the computation of each load impedance and the corresponding feeding voltage are given;
2) We formulate the relationship between the current vector with quantized loads and the ideal current vector. We then mathematically analyze the performance of precoding schemes for ESPAR based MIMO systems with quantized loads for both perfect CSI and imperfect CSI, where it is shown that the presence of quantized loads introduces an additional noise term that is independent of the transmit SNR, which then leads to an error floor at high SNR regime;
3) We obtain a closed-form solution to approximate the current vector of the ESPAR array to the desired signal

vector based on convex optimization to compensate for the performance loss introduced by the quantized loads, where it is proven that the optimality is achieved by optimizing the feeding voltage only while keeping the values of each tunable load unchanged.

The rest of the paper is organized as follows: Section II introduces the system model for ESPAR and the correlated channel model. Section III introduces the extension of existing precoding schemes to single-fed ESPAR MIMO systems, where the calculation of each load impedance and the corresponding feeding voltage is given. Section IV analyzes the system performance for ESPARs with quantized load impedances for both perfect CSI and imperfect CSI. Section V introduces the proposed scheme based on convex optimization to compensate for the performance loss introduced by the quantized loads, and Section VI discusses the practical implementations of the ESPAR-based MIMO systems. Section VII introduces the energy efficiency measurement. Section VIII presents the numerical results and Section IX concludes our paper.

Notations: $\mathrm{E}(\cdot)$, $(\cdot)^*$, $(\cdot)^T$, $(\cdot)^H$, $(\cdot)^{-1}$, and $tr(\cdot)$ denote the expectation, conjugate, transpose, conjugate transpose, inverse, and trace of a matrix respectively. $\|\cdot\|$ denotes the Frobenius norm, $\mathbf{I}$ is the identity matrix and $\mathbf{0}$ denotes a zero matrix or vector. $\mathcal{C}^{n\times n}$ represents $n\times n$ matrix in the complex set and $\mathbf{R}(k,u)$ denotes the element of the kth-row and uth-column in $\mathbf{R}$. $diag(\cdot)$ denotes the conversion of a vector into a diagonal matrix with the values on its main diagonal. $\Re(\cdot)$ denotes the real part and $\Im(\cdot)$ denotes the imaginary part of a complex variable, respectively.

II. System Model

In this section, the considered signal model which captures the features of ESPAR antennas is given, followed by the MIMO system description and the correlated channel model we consider.

A. Signal Model

We first consider the signal model for the conventional antenna array, and then extend to single-fed ESPARs. Assume that an AP is equipped with N_t antennas, and each antenna $k \in \{1,2,...,N_t\}$ is fed by an independent source with the complex voltage v_k and the output impedance z_0, where the equivalent circuit representation is shown in Fig. 1 (a). We denote the mutual impedance matrix of the transmit array as $\mathbf{Z}_m \in \mathcal{C}^{N_t\times N_t}$, which is related to the carrier frequency and the antenna spacing. Then, according to the generalized Ohm's law, the complex current vector at the antenna port can be expressed as [21]

$$\mathbf{i}_0 = [diag(\mathbf{z}_0) + \mathbf{Z}_m]^{-1}\mathbf{v}_0, \tag{1}$$

where $\mathbf{i}_0 \in \mathcal{C}^{N_t\times 1}$ is the current vector, $\mathbf{z}_0 \in \mathcal{C}^{N_t\times 1}$ is output impedance vector, and $\mathbf{v}_0 \in \mathcal{C}^{N_t\times 1}$ is the voltage vector. We note that for a conventional MIMO array each element in $\mathbf{z}_0$ is fixed as z_0 (which usually equals 50Ω), and each element in $\mathbf{v}_0$ is non-zero and adjusted based on the desired signal vector.

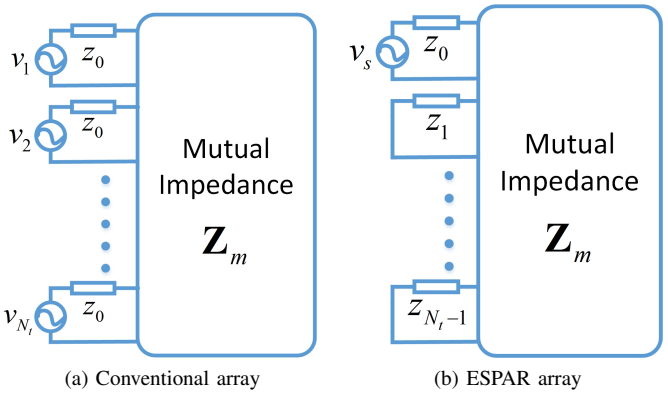

(a) Conventional array (b) ESPAR array

Fig. 1: Circuit representation

When the AP is equipped with a single-fed ESPAR array, the circuit representation is shown in Fig. 1 (b), where only the central active element is fed with the voltage v_s, while the remaining N_t-1 elements are parasitic and excited passively by the mutual coupling effect between antenna elements. In this case, the current vector at the antenna port can be obtained based on (1) as [23]

$$\begin{aligned}\mathbf{i} &= [diag(\mathbf{z}_L) + \mathbf{Z}_m]^{-1}\cdot[v_s,0,....,0]^T \\ &= [diag(\mathbf{z}_L) + \mathbf{Z}_m]^{-1}\mathbf{v}_s \\ &= \mathbf{Z}_T\mathbf{v}_s,\end{aligned} \tag{2}$$

where $\mathbf{z}_L = [z_0, z_1, z_2, ..., z_{N_t-1}]^T$ is the load impedance vector and we denote $\mathbf{Z}_T$ as the effective coupling matrix. z_0 is the fixed load impedance that corresponds to the active antenna element, and each z_i, $i \in \{1,2,...,N_t-1\}$ is the tunable load that is connected to each parasitic antenna element to control the radiation pattern for ESPARs. As observed from (2), different from conventional antenna array where the current on each antenna is controlled by each voltage source, for ESPARs the effective coupling matrix $\mathbf{Z}_T$ is controlled by tuning each value of z_i, and the currents at each antenna port can then be controlled accordingly.

In this paper we consider a multi-user case, where the AP equipped with an ESPAR antenna array communicates with a total number of K single-antenna users in the system. Then, based on the proposition in [23][24][31], we can consider the current vector at the antenna port of the ESPAR array as the input, and a general system equation that captures the functionality of an antenna array can be expressed as

$$\mathbf{y} = \mathbf{H}\mathbf{i} + \mathbf{n}, \tag{3}$$

where $\mathbf{y} \in \mathcal{C}^{K\times 1}$ denotes the received signal vector, $\mathbf{H} \in \mathcal{C}^{K\times N_t}$ is the channel matrix, $\mathbf{n} \in \mathcal{C}^{K\times 1}$ denotes the additive white Gaussian noise (AWGN) vector and $\mathbf{n} \sim \mathcal{CN}\left(0, \sigma^2\cdot\mathbf{I}\right)$, where σ^2 is the noise power.

In conventional MIMO systems, the transmitting and receiving signals indeed relate to the amplitude and phase of the observed quantity which can be the voltage or current vector. In this case, the channel matrix typically relates the 'input voltages' and the 'output voltages'. On the other hand, when

mutual coupling is considered even in a conventional MIMO system, the relationship between the currents and the feeding voltages, as given by (1) of our paper, is required with each entry of $\mathbf{v}_0$ being non-zero [20]-[26]. While (1) is applicable for both conventional MIMO and ESPAR MIMO, conventional MIMO systems typically assume an antenna spacing of $\lambda/2$ or even larger to avoid the mutual coupling effect in practice, in which case the mutual coupling effect can be neglected, and therefore the mutual impedance matrix becomes a diagonal matrix, which leads to $Z_m = z_c \cdot \mathbf{I}$ where z_c denotes the common self-impedance to match the voltage source. Then, the current vector is further obtained as $\mathbf{i}_0 = (z_0 + z_c)^{-1} \cdot \mathbf{v}_0$, i.e., the currents on each antenna port are a scaled version of the feeding voltages. Then, the channel that relates the 'input currents' and the 'output voltages' can be regarded as a scaled version of the conventional channel matrix, while the statistical properties remain the same. In other words, the channel model developed for conventional MIMO is also valid to relate 'input currents' and 'output voltages'. Therefore, for the ESPAR-based MIMO systems where the input is given by (2), current channel models for conventional MIMO systems can be directly applied to relate 'input currents' and 'output voltages'.

B. Channel Model

Compared to conventional antenna array that has a relatively large antenna spacing to avoid mutual coupling effect, the antenna spacing for ESPARs is small, as the currents on each parasitic antennas are passively excited by the mutual coupling effect between antenna elements. Therefore, the channel model for ESPARs must take the correlation effect among antenna elements into consideration, which is then modeled as a geometric semi-correlated Rayleigh flat fading channel, given by [32][33]

$$\mathbf{H} = \left[\mathbf{h}_1^T, ..., \mathbf{h}_k^T, ..., \mathbf{h}_K^T\right]^T, \tag{4}$$

with the $1 \times N_t$ channel vector $\mathbf{h}_k$ for the k-th user being

$$\mathbf{h}_k = \mathbf{g}_k \mathbf{A}_k, \tag{5}$$

where $\mathbf{g}_k \in \mathcal{C}^{1\times M}$ and M denotes the number of directions of departure (DoDs). Each element in $\mathbf{g}_k$ is distributed as $\mathcal{CN}(0,1)$ that forms the Rayleigh component. $\mathbf{A}_k \in \mathcal{C}^{M\times N_t}$ represents the transmit-side steering matrix that contains M steering vectors of the transmit antenna array. For uniform linear arrays (ULAs), as assumed in this paper, $\mathbf{A}_k$ can be expressed as

$$\mathbf{A}_k = \frac{1}{\sqrt{M}}\left[\mathbf{a}^T(\theta_{k,1}), ..., \mathbf{a}^T(\theta_{k,M})\right]^T, \tag{6}$$

where $\mathbf{a}(\theta_{k,i}) \in \mathcal{C}^{1\times N_t}$ is given by

$$\mathbf{a}(\theta_{k,i}) = \left[1, e^{j2\pi d \sin\theta_{k,i}}, ..., e^{j2\pi(N_t-1)d\sin\theta_{k,i}}\right]. \tag{7}$$

In (7), d denotes the equidistant antenna spacing normalized by the carrier wavelength. $\theta_{k,i}$ denotes the angle of departure (AoDs) and throughout the paper we assume each $\theta_{k,i}$ follows a uniform distribution in $[-\pi, \pi]$. It is worth noting that for a compact antenna array, the mutual coupling effect should also be considered in the channel model. For the ESPAR array, we note that the mutual coupling effect has been taken into account by the mutual impedance matrix $\mathbf{Z}_m$ and further $\mathbf{Z}_T$ when calculating the currents in (2), and is therefore not explicitly shown in the channel model. By substituting (2) into (3), the received signals can be obtained as

$$\mathbf{y} = \mathbf{H}\underbrace{\mathbf{Z}_T\mathbf{v}_s}_{\mathbf{i}} + \mathbf{n}. \tag{8}$$

As can be seen in (8), the above channel model considers both the correlation and mutual coupling effect at the AP. For the purpose of the analysis below, full knowledge of channel state information (CSI) is firstly assumed at the AP, which is a common assumption for precoding schemes, while cases with imperfect CSI are also investigated in the following section.

III. Extension of Precoding Schemes to ESPARs

In conventional MIMO systems, precoding schemes employ the knowledge of the channel matrix to form the precoding matrix. In a $K \times N_t$ MU-MISO system, the precoded signal vector can be expressed as

$$\mathbf{x} = f \cdot \mathbf{P}\mathbf{s}, \tag{9}$$

where $\mathbf{s} \in \mathcal{C}^{K\times 1}$ is data symbol vector, and $\mathbf{P}$ is the precoding matrix. f is the scaling factor that ensures the signal power to remain unchanged after precoding, which is given by

$$f = \frac{1}{\sqrt{tr\left(\mathbf{P}^H\mathbf{P}\right)}}. \tag{10}$$

In order to apply the precoding schemes for ESPAR based MIMO systems, the precoded signal vector is mapped to the antenna current vector [24][31], i.e.,

$$\mathbf{i} = \mathbf{x} = f \cdot \mathbf{P}\mathbf{s}. \tag{11}$$

Then, (3) is transformed into

$$\mathbf{y} = f \cdot \mathbf{H}\mathbf{P}\mathbf{s} + \mathbf{n}. \tag{12}$$

With this approach, ESPARs can form the same transmit signal and radiate as conventional MIMO. Then, we need to obtain the values of each tunable load z_i, $i \in \{1, 2, ..., N_t - 1\}$ and the corresponding feeding voltage v_s that form the desired radiation pattern. We rewrite (2) and expand it in (13) which is shown on the top of next page. Then, based on (13), the feeding voltage and the value of each tunable loads can be calculated as [23][24]

$$\begin{aligned} v_s &= \sum_{m=1}^{N_t} \mathbf{Z}_m(1,m)\, i_m + z_0 i_1, \\ z_k &= -\frac{1}{i_{k+1}} \sum_{m=1}^{N_t} \mathbf{Z}_m(k+1,m)\, i_m,\ k \in \{1, 2, ..., N_t - 1\}. \end{aligned} \tag{14}$$

As mentioned earlier, the currents are dependent on the precoding schemes and the symbols that are known before transmission. Therefore, by setting the feeding voltage and the loads as calculated based on (14), the ESPARs can radiate

$$\begin{bmatrix} \mathbf{Z}_m(1,1)+z_0 & \mathbf{Z}_m(1,2) & \cdots & \mathbf{Z}_m(1,N_t) \\ \mathbf{Z}_m(2,1) & \mathbf{Z}_m(2,2)+z_1 & \ddots & \mathbf{Z}_m(2,N_t) \\ \vdots & \ddots & \ddots & \vdots \\ \mathbf{Z}_m(N_t,1) & \mathbf{Z}_m(N_t,2) & \cdots & \mathbf{Z}_m(N_t,N_t)+z_{N_t-1} \end{bmatrix} \begin{bmatrix} i_1 \\ i_2 \\ \vdots \\ i_{N_t} \end{bmatrix} = \begin{bmatrix} v_s \\ 0 \\ \vdots \\ 0 \end{bmatrix} \tag{13}$$

the desired signals as conventional MIMO. Different from conventional MIMO, due to the existence of the tunable loads the input impedance of ESPAR based array is dependent on the current vector on each port, which is given by

$$z_{in} = \mathbf{Z}_m(1,1) + \sum_{m=2}^{N_t} \mathbf{Z}_m(1,m) \cdot \frac{i_m}{i_1}. \tag{15}$$

As can be observed in (15), an arbitrary current vector at the antenna port may lead to $\Re(z_{in}) < 0$. In such case, the ESPAR array is unable to radiate power and will instead consume power. $\Re(z_{in}) > 0$ can be satisfied by designing $\mathbf{Z}_m$ with a large enough $\mathbf{Z}_m(1,1)$.

IV. Performance Analysis for ESPARs with Quantized Loads and Imperfect CSI

A. ESPARs with Quantized Loads

It is observed from (14) that the calculation of each tunable load and the feeding voltage is based on the assumption that each parasitic load has a continuous value range and can be tuned to any arbitrary values. However, this may be infeasible in practice, and due to the realistic hardware implementation quantized loads are employed in most cases [34]-[36]. Therefore in this section, we study the impact of the quantization in each tunable load on the system performance of ESPARs. Then, we can express the value of each quantized load as

$$\hat{z}_k = z_k + e_k^l,\ k \in \{1,2,...,N_t-1\}, \tag{16}$$

where $\hat{z}_k$ denotes the quantized load at the k-th passive antenna in practice, z_k denotes the ideal load impedace value that forms the desired radiation pattern, and e_k^l is the error in the load value. For the quantized loads, we denote D as the quantization level for both the real part and imaginary part of the load impedance, and in this case the potential values of the quantized loads can be obtained as

$$\hat{z}_k = m_k D + j \cdot n_k D,\ m_k, n_k \in \{0, \pm 1, \pm 2, ...\}. \tag{17}$$

Due to the quantization, the impedance error e_k^l for each tunable load can be regarded as a variable that is norm bounded, and the bound that is related to the quantization level can be obtained as

$$\left\|e_k^l\right\|^2 \leq \left(\frac{D}{2}\right)^2 + \left(\frac{D}{2}\right)^2 = \frac{D^2}{2}. \tag{18}$$

B. Performance Analysis - Quantized Loads, Perfect CSI

Before we begin to study the effect of quantized loads on the system performance of ESPARs, firstly we need to study the correlated channel $\mathbf{H}$. Recall (5)(6) and notice that the transposition does not have an impact on the variable distribution, we can then obtain

$$\mathbf{h}_k^T = \left(\mathbf{g}_k \mathbf{A}_k\right)^T = \mathbf{A}_k^T \mathbf{g}_k^T, \tag{19}$$

where $\mathbf{A}_k^T \in \mathcal{C}^{N_t \times M}$ and $\mathbf{g}_k^T \in \mathcal{C}^{M \times 1}$.

Lemma: For a random variable $\mathbf{z} \sim \mathcal{CN}(\mathbf{0}, \mathbf{K}_z)$, if there exists a linear transformation $\mathbf{y} = \mathbf{Bz}$, then we have $\mathbf{y} \sim \mathcal{CN}\left(\mathbf{0}, \mathbf{B}\mathbf{K}_z\mathbf{B}^H\right)$ [37].

Based on the lemma given above and noting that the elements of $\mathbf{g}_k^T$ are complex random variables with standard complex Gaussian distribution, the elements of $\mathbf{h}_k$ also follow the Gaussian distribution with zero mean, and the covariance matrix is given by

$$\mathbf{C}_{\mathbf{h}_k^T} = \mathbf{A}_k^T \left(\mathbf{A}_k^T\right)^H = \mathbf{A}_k^T \mathbf{A}_k^*, \tag{20}$$

With the above analysis, each row of $\mathbf{H}$ is proved to follow a normal distribution with zero mean and the covariance matrix given by (20). It should be noted that for each user k, $\mathbf{A}_k$ is slightly different from each other, and for tractability of analysis we apply the average of $\mathbf{A}_k$ to obtain the covariance matrix of $\mathbf{H}$, denoted as $\mathbf{C}_{\mathbf{H}}$.

We then focus on the performance analysis of ESPARs for perfect CSI cases with the the errors in the load impedances only. Consider each tunable load value with error e_k^l as in (16), then the current vector in (2) with quantized loads can be rewritten as

$$\begin{aligned} \hat{\mathbf{i}} &= \left[diag\left(\hat{\mathbf{z}}_L\right) + \mathbf{Z}_m\right]^{-1} \mathbf{v}_s \\ &= \left[diag\left(\mathbf{z}_L\right) + \mathbf{E}_l + \mathbf{Z}_m\right]^{-1} \mathbf{v}_s \\ &= \left(\mathbf{Z}_T^{-1} + \mathbf{E}_l\right)^{-1} \mathbf{v}_s, \end{aligned} \tag{21}$$

where $\hat{\mathbf{z}}_L$ is the quantized load impedance vector and $\mathbf{E}_l = diag\left(0, e_1^l, ..., e_{N_t-1}^l\right)$ is the impedance error matrix. In ideal cases where the parasitic loads with continuous values are employed, the feeding voltage can be calculated as (14) and in cases with impedance errors, the feeding voltage remains the same. In this case, we have

$$\left(\mathbf{Z}_T^{-1} + \mathbf{E}_l\right) \hat{\mathbf{i}} = \mathbf{Z}_T^{-1} \mathbf{i}. \tag{22}$$

Then, the current vector with quantized impedance errors can be further transformed into

$$\begin{aligned} \hat{\mathbf{i}} &= \left(\mathbf{Z}_T^{-1} + \mathbf{E}_l\right)^{-1} \mathbf{Z}_T^{-1} \mathbf{i} \\ &= \left(\mathbf{Z}_T^{-1} + \mathbf{E}_l\right)^{-1} \left(\mathbf{Z}_T^{-1} + \mathbf{E}_l - \mathbf{E}_l\right) \mathbf{i} \\ &= \mathbf{i} - \left(\mathbf{Z}_T^{-1} + \mathbf{E}_l\right)^{-1} \mathbf{E}_l \mathbf{i}. \end{aligned} \tag{23}$$

Then, the received signal vector in the presence of the impedance errors can be obtained by substituting (23) into (3), expressed as

$$\begin{aligned}\mathbf{y} &= \mathbf{H}\hat{\mathbf{i}} + \mathbf{n} \\ &= \mathbf{H}\left[\mathbf{i} - \left(\mathbf{Z}_T^{-1} + \mathbf{E}_l\right)^{-1}\mathbf{E}_l\mathbf{i}\right] + \mathbf{n} \\ &= \mathbf{H}\mathbf{i} - \mathbf{H}\left(\mathbf{Z}_T^{-1} + \mathbf{E}_l\right)^{-1}\mathbf{E}_l\mathbf{i} + \mathbf{n} \\ &= \mathbf{H}\mathbf{i} + \mathbf{n}_l + \mathbf{n}.\end{aligned} \tag{24}$$

Compared to (3), the second term $\mathbf{n}_l$ introduced by the impedance errors due to quantization can be regarded as an additional noise term that is independent of the transmit SNR. We then define the equivalent noise term

$$\begin{aligned}\mathbf{n}_e &\triangleq \mathbf{n}_l + \mathbf{n} \\ &= -\mathbf{H}\left(\mathbf{Z}_T^{-1} + \mathbf{E}_l\right)^{-1}\mathbf{E}_l\mathbf{i} + \mathbf{n}.\end{aligned} \tag{25}$$

We note that the errors here are introduced by the quantization in the load impedances, and therefore the AP has the knowledge of the error matrix $\mathbf{E}_l$. Then, based on (25), it can be observed that $\mathbf{n}_e$ conditioned on $\mathbf{H}$ and $\mathbf{i}$ follows an i.i.d. Gaussian distribution with zero mean [38], where the equivalent noise power for each user k is given by

$$\upsilon_k = \omega_k \zeta^2 \delta_k + \sigma^2. \tag{26}$$

In (26), $\omega_k = \frac{1}{N_t}\|\mathbf{C_H}\|^2$ where $\mathbf{C_H}$ is the channel covariance matrix, $\zeta = \left\|\left(\mathbf{Z}_T^{-1} + \mathbf{E}_l\right)^{-1}\right\|$ represents the effect of the antenna coupling, and $\delta_k = \left\|e_k^l\right\|^2$. The current vector is equal to the normalized transmit signal vector and then we have $\|\mathbf{i}\|^2 = 1$. Furthermore, note that each e_k^l is norm bounded as shown in (18), we can similarly obtain the upper bound of the equivalent noise power as

$$\upsilon_{upper} = \frac{\varpi \zeta^2 D^2}{2} + \sigma^2, \tag{27}$$

where ϖ is the average over ω_k.

We note that the above derivation is independent of the precoding schemes applied at the AP. To obtain the received SNR and the resulting analytical probability of error, in the following we assume that CI precoding is employed at the AP, where based on (11) the current vector can be expressed as

$$\mathbf{i} = f \cdot \mathbf{H}^H\left(\mathbf{H}\mathbf{H}^H\right)^{-1}\mathbf{s}, \tag{28}$$

and the scaling factor $f = \sqrt{1 \Big/ tr\left[\left(\mathbf{H}^H\mathbf{H}\right)^{-1}\right]}$. Then, the received signal vector with quantized loads is obtained as

$$\begin{aligned}\mathbf{y} &= \mathbf{H} \cdot f \cdot \mathbf{H}^H\left(\mathbf{H}\mathbf{H}^H\right)^{-1}\mathbf{s} + \mathbf{n}_e \\ &= f \cdot \mathbf{s} + \mathbf{n}_e,\end{aligned} \tag{29}$$

and then the resulting received SNR is given by

$$\gamma_k = f^2 \cdot \frac{\|s_i\|^2}{\omega_k \zeta^2 \delta_k + \sigma^2}. \tag{30}$$

It is then observed that the first term of the noise is irrelevant to the transmit SNR, and therefore at high transmit SNR regime where σ^2 becomes negligible, an error floor will be observed.

Probability of error: In order to validate our analysis, we introduce the probability of bit error for QPSK in flat fading with respect to the transmit SNR for $K = N_t$, and the average bit error rate (BER) over all MIMO streams can be calculated as [39]-[41]

$$P_e = \frac{1}{2K}\sum_{k=1}^{K}\left[1 - \sqrt{\frac{\rho_k}{\tau_k^2 + \rho_k}}\right], \tag{31}$$

where $\tau_k^2 = \mathbf{C}_{\mathbf{H}}^{-1}(k,k)$ is the k-th diagonal element in the inverse matrix of the channel covariance $\mathbf{C_H}$. ρ_k is the signal-to-noise ratio per bit (E_bN_0) for stream k. For CI precoding, ρ_i for each stream can be obtained based on γ_k, expressed as

$$\rho_k = \frac{1}{2K\left(\omega_k \zeta^2 \delta_k + \sigma^2\right)}. \tag{32}$$

Similarly, based on the upper bound of the noise power in (27) we can obtain the lower bound of ρ_k, which is expressed as

$$\rho_k \geq \frac{1}{2K\left(\frac{\varpi \zeta^2 D^2}{2} + \sigma^2\right)} \triangleq \rho_k^{lower}. \tag{33}$$

Fig. 2 compares the analytical BER and the numerical results for CI precoding under perfect CSI, where for the considered system the number of DoDs is $M = 50$ and we assume $K = N_t = 5$, i.e. ESPAR has a ULA structure with the active antenna at the center and four parasitic antennas, two at each side, and there is a total number of $K = 5$ users in the system. For simplicity, we assume $P = 1$ and the quantization level is $D = 1$. The system operates at frequency $f = 2.5$GHz and the spacing between ESPAR antennas is assumed as $d = 0.25$, which is equivalent to $\lambda/4$. A relatively large value $(465.4 - 659.5i)\Omega$ is chosen as the antenna impedance to ensure a positive real part of the input impedance. The mutual impedance can be calculated with the electromagnetic-field (EMF) methods based on the antenna spacing d [42]. We summarize the simulation parameters in Table I. For clarity the following abbreviations are used throughout the paper:

1) "MIMO CI": conventional MIMO CI precoding;
2) "ESPAR CI ideal": simulated ESPAR CI precoding with ideal loads;
3) "ESPAR CI Quantized": simulated ESPAR CI precoding with quantized loads;
4) "ESPAR CI Analytical": analytical BER result of ESPAR CI precoding with quantized loads by (32);
5) "ESPAR CI Upperbound": the BER upper bound of ESPAR CI precoding with quantized loads by (33).

It can be seen that with ideal continuous loads, ESPAR-based MIMO systems with a single RF chain can achieve the same performance as conventional MIMO with a full number of RF

Simulation parameters	Values
Operating frequency	2.5GHz
Antenna spacing d	$\lambda/4$
Number of DoDs M	50
Quantization level D	1
Number of active antennas	1
Number of parasitic antennas	4

TABLE I: Simulation Parameters

chains. When we employ the practical quantized loads, it is observed that ESPAR suffers a performance degradation and an error floor appears at high SNR regime. It is also observed that the analytical BER performance matches the simulated result.

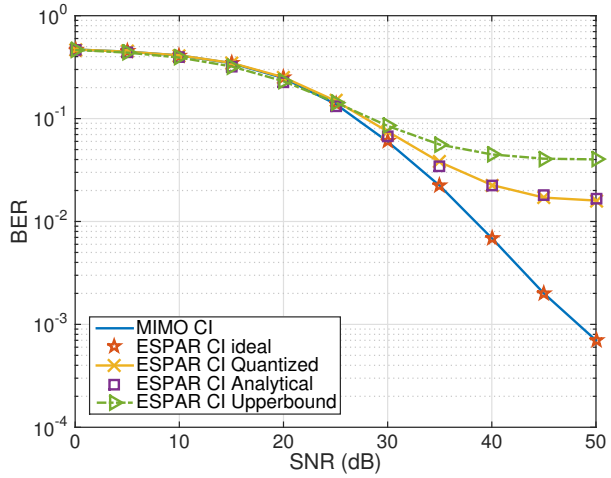

Fig. 2: BER performance of MIMO and ESPAR-based MIMO, perfect CSI, $N_t = K = 5$, $D = 1$, QPSK

C. Performance Analysis - Quantized Loads, Imperfect CSI

We then proceed to investigate the imperfect CSI model and the performance of ESPAR-based MIMO system under scenarios with imperfect CSI and quantized loads. In this paper, we assume that the system is operating in TDD mode and therefore the CSI $\hat{\mathbf{H}}$ is directly measured at the transmitter using uplink-downlink reciprocity and is subject to noise errors [43]. Then, the errors are modeled as inversely proportional to the transmit SNR, expressed as

$$\mathbf{H} = \hat{\mathbf{H}} + \mathbf{Q}, \tag{34}$$

where $\mathbf{H}$ represents the channel at transmission and $\hat{\mathbf{H}}$ is the estimated channel, with the error matrix $\mathbf{Q} \sim \mathcal{CN}(0, \eta \cdot \mathbf{I}_{N_t})$ that is statistically independent of $\hat{\mathbf{H}}$. η is the variance of the channel error and is obtained as

$$\eta = \beta \cdot \left(\frac{1}{\sigma^2}\right)^{-1}, \tag{35}$$

where β is the inverse proportionality coefficient, with $\frac{1}{\sigma^2}$ being the transmit SNR.

With the imperfect CSI model above, by substituting (23) and (34) into (3), the received signals can be obtained as

$$\begin{aligned}\mathbf{y} &= \mathbf{H}\left[\mathbf{i} - \left(\mathbf{Z}_T^{-1} + \mathbf{E}_l\right)^{-1}\mathbf{E}_l\mathbf{i}\right] + \mathbf{n} \\ &= \left(\hat{\mathbf{H}} + \mathbf{Q}\right)\mathbf{i} - \left(\hat{\mathbf{H}} + \mathbf{Q}\right)\left(\mathbf{Z}_T^{-1} + \mathbf{E}_l\right)^{-1}\mathbf{E}_l\mathbf{i} + \mathbf{n} \\ &= \hat{\mathbf{H}}\mathbf{i} + \mathbf{Q}\mathbf{i} - \left(\hat{\mathbf{H}} + \mathbf{Q}\right)\left(\mathbf{Z}_T^{-1} + \mathbf{E}_l\right)^{-1}\mathbf{E}_l\mathbf{i} + \mathbf{n},\end{aligned} \tag{36}$$

Then, we can similarly define the equivalent noise term for imperfect CSI as

$$\hat{\mathbf{n}}_e \triangleq \mathbf{Q}\mathbf{i} - \left(\hat{\mathbf{H}} + \mathbf{Q}\right)\left(\mathbf{Z}_T^{-1} + \mathbf{E}_l\right)^{-1}\mathbf{E}_l\mathbf{i} + \mathbf{n}. \tag{37}$$

Compared to the case of perfect CSI, we observe that an additional noise term $\mathbf{Q}\mathbf{i}$ is introduced as a result of the imperfect CSI. Then, $\hat{\mathbf{n}}_e$ conditioned on $\mathbf{Q}$, $\mathbf{H}$ and $\mathbf{i}$ is i.i.d. Gaussian with zero mean, and the equivalent noise power for the kth user is given by

$$\hat{\upsilon}_k = \eta + \hat{\omega}_k\zeta^2\delta_k + \sigma^2, \tag{38}$$

where $\hat{\omega}_k = \frac{1+\eta}{N_t}\|\mathbf{C}_\mathbf{H}\|^2$ considers the channel estimation error effect on the coupling matrix. The upper bound of the equivalent noise power for imperfect CSI can be further obtained as

$$\hat{\upsilon}_{upper} = \eta + \frac{\hat{\varpi}\zeta^2 D^2}{2} + \sigma^2, \tag{39}$$

where $\hat{\varpi}$ is the average of $\hat{\omega}_k$.

Probability of error: Under imperfect CSI, the analytical BER is also obtained from (31). Assuming CI precoding at the transmitter, we can similarly express the E_bN_0 for each user k with imperfect CSI as

$$\hat{\rho}_k = \frac{1}{2K\left(\eta + \hat{\omega}_k\zeta^2\delta_k + \sigma^2\right)}. \tag{40}$$

Then, based on the equivalent upper bound of the noise power, we can obtain the lower bound of the E_bN_0 for imperfect CSI, expressed as

$$\hat{\rho}_k \geq \frac{1}{2K\left(\eta + \frac{\hat{\varpi}\zeta^2 D^2}{2} + \sigma^2\right)} \triangleq \hat{\rho}_k^{lower}. \tag{41}$$

In order to validate the analysis, Fig. 3 shows the BER performance of the ESPAR based MIMO systems with quantized loads under imperfect CSI. The channel error coefficient is assumed to be $\beta = 2.5$. It is observed that while a similar BER trend can be observed compared to Fig. 2 where CSI is perfect and there only exist quantization errors, the performance is degraded due to the channel estimation errors. It is also observed that under imperfect CSI, the analytical BER performance matches the simulated result.

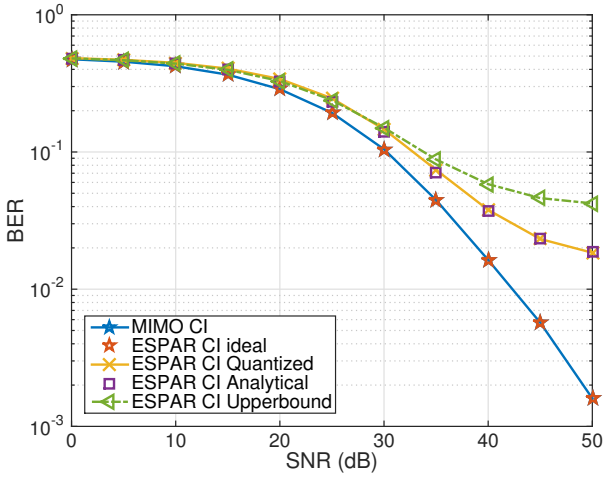

Fig. 3: BER performance of MIMO and ESPAR-based MIMO, imperfect CSI, $N_t = K = 5$, $D = 1$, $\beta = 2.5$, QPSK

V. Proposed Quantization-Robust Scheme

As noted above, the presence of the quantized loads leads to a performance loss for the ESPAR array at high SNR regime. Therefore in this section we propose to compensate for this loss by approximating the current vector of ESPARs to the desired signal vector with convex optimization. Specifically, we propose to jointly optimize the feeding voltage and the quantized loads such that an improved performance can be achieved, which is introduced in detail in the following.

In the presence of the variation in the quantized loads and the feeding voltage, based on (2) the current vector for the ESPAR array can be expressed as

$$\begin{aligned}\tilde{\mathbf{i}} &= \left[diag\left(\tilde{\mathbf{z}}_L\right) + \mathbf{Z}_m\right]^{-1}\tilde{\mathbf{v}}_s \\ &= \left[diag\left(\mathbf{z}_L\right) + \mathbf{Z}_m + \tilde{\mathbf{E}}_l\right]^{-1}\left(\mathbf{v}_s + \Delta\mathbf{v}\right),\end{aligned} \tag{42}$$

where $\tilde{\mathbf{z}}_L$ denotes the optimized quantized loads, $\tilde{\mathbf{v}}_s$ is the optimized feeding voltage and $\Delta\mathbf{v}$ denotes the variation in the feeding voltage. The variation in the load impedances $\tilde{\mathbf{E}}_l$ can be further expressed as

$$\tilde{\mathbf{E}}_l = \mathbf{E}_l + D \cdot diag\left(\mathbf{t}\right), \tag{43}$$

where $\mathbf{E}_l$ is given in (21) and $\mathbf{t} \in \mathcal{CZ}^{N_t \times 1}$ with each element being a complex integer. $D \cdot diag\left(\mathbf{t}\right)$ then denotes the additional quantized load impedance values compared to $\mathbf{E}_l$ in the case of optimality. Note that for single-fed ESPAR arrays, only the active central antenna element is fed with the voltage, and therefore only one entry is non-zero for both $\mathbf{v}_s$ and $\Delta\mathbf{v}$. Then, by introducing an auxiliary complex variable α where

$$\Delta\mathbf{v} = \alpha \cdot \mathbf{v}_s, \tag{44}$$

(42) can be further transformed into

$$\begin{aligned}\tilde{\mathbf{i}} &= \left[diag\left(\tilde{\mathbf{z}}_L\right) + \mathbf{Z}_m\right]^{-1}\left(1+\alpha\right)\mathbf{v}_s \\ &= \left(1+\alpha\right)\left[diag\left(\tilde{\mathbf{z}}_L\right) + \mathbf{Z}_m\right]^{-1}\left[diag\left(\mathbf{z}_L\right) + \mathbf{Z}_m\right]\mathbf{i} \\ &= \left(1+\alpha\right)\left\{\mathbf{i} - \left[diag\left(\tilde{\mathbf{z}}_L\right) + \mathbf{Z}_m\right]^{-1}\tilde{\mathbf{E}}_l\mathbf{i}\right\} \\ &= \left(1+\alpha\right)\left\{\mathbf{i} - \left[diag\left(\tilde{\mathbf{z}}_L\right) + \mathbf{Z}_m\right]^{-1}\left[\mathbf{E}_l + D \cdot diag\left(\mathbf{t}\right)\right]\mathbf{i}\right\}.\end{aligned} \tag{45}$$

Then, based on (45), we can express the difference between the optimized current vector and the desired current vector as

$$\begin{aligned}\Delta\mathbf{i} =& \tilde{\mathbf{i}} - \mathbf{i} \\ =& \alpha\mathbf{i} - \left(1+\alpha\right)\left[diag\left(\tilde{\mathbf{z}}_L\right) + \mathbf{Z}_m\right]^{-1}\left[\mathbf{E}_l + D \cdot diag\left(\mathbf{t}\right)\right]\mathbf{i} \\ =& \Big\{\alpha\mathbf{I} - \left(1+\alpha\right)\left[diag\left(\mathbf{z}_L\right) + \mathbf{Z}_m + \mathbf{E}_l + D \cdot diag\left(\mathbf{t}\right)\right]^{-1} \\ & \left[\mathbf{E}_l + D \cdot diag\left(\mathbf{t}\right)\right]\Big\}\mathbf{i}.\end{aligned} \tag{46}$$

By denoting

$$\mathbf{A} = diag\left(\mathbf{z}_L\right) + \mathbf{Z}_m + \mathbf{E}_l, \tag{47}$$

which is fixed in terms of the optimization variables, (46) is further transformed into

$$\begin{aligned}&\Delta\mathbf{i} \\ =& \left\{\alpha\mathbf{I} - \left(1+\alpha\right)\left[\mathbf{A} + D \cdot diag\left(\mathbf{t}\right)\right]^{-1}\left[\mathbf{E}_l + D \cdot diag\left(\mathbf{t}\right)\right]\right\}\mathbf{i} \\ =& \left\{\alpha\mathbf{I} - \left(1+\alpha\right)\mathbf{I} - \left(1+\alpha\right)\left[\mathbf{A} + D \cdot diag\left(\mathbf{t}\right)\right]^{-1}\left(\mathbf{E}_l - \mathbf{A}\right)\right\}\mathbf{i} \\ =& \left\{-\mathbf{I} + \left(1+\alpha\right)\left[\mathbf{A} + D \cdot diag\left(\mathbf{t}\right)\right]^{-1}\left(\mathbf{A} - \mathbf{E}_l\right)\right\}\mathbf{i}.\end{aligned} \tag{48}$$

We can then formulate the optimization problem as

$$\begin{aligned}\mathcal{P}_0: \ &\min_{\alpha,\,\mathbf{t}} \ \left\|\Delta\mathbf{i}\right\|^2 \\ &s.t. \\ &\mathbf{t}\left(1\right) = 0\end{aligned} \tag{49}$$

The constraint here corresponds to the active antenna element where the load impedance is constant. Based on the structure of $\Delta\mathbf{i}$ shown in (48), the following proposition is obtained.

Proposition 1: $\Delta\mathbf{i}$ cannot be minimized to 0 by optimizing α which corresponds to the feeding voltage and $\mathbf{t}$ which corresponds to the quantized loads.

Proof: Based on (48), to have $\left\|\Delta\mathbf{i}\right\|^2 = 0$ for any current vector $\mathbf{i}$ is equivalent to

$$\left(1+\alpha\right)\left[\mathbf{A} + D \cdot diag\left(\mathbf{t}\right)\right]^{-1}\left(\mathbf{A} - \mathbf{E}_l\right) = \mathbf{I}, \tag{50}$$

which can be further transformed into

$$\begin{aligned}&\mathbf{A} + D \cdot diag\left(\mathbf{t}\right) = \left(1+\alpha\right)\left(\mathbf{A} - \mathbf{E}_l\right) \\ \Rightarrow\ & D \cdot diag\left(\mathbf{t}\right) = \alpha\mathbf{A} - \left(1+\alpha\right)\mathbf{E}_l \\ \Rightarrow\ & diag\left(\mathbf{t}\right) = \frac{1}{D} \cdot \left[\alpha\mathbf{A} - \left(1+\alpha\right)\mathbf{E}_l\right].\end{aligned} \tag{51}$$

From (51), if $\alpha = 0$, then $diag\left(\mathbf{t}\right) = -\frac{1}{D} \cdot \mathbf{E}_l$. Since $\mathbf{E}_l$ is the diagonal impedance error matrix due to quantization, based on (18) the absolute value of both the real part and the imaginary part of e_k^l, i.e. each diagonal element in $\mathbf{E}_l$, is smaller than D. Since $\mathbf{t}$ is the complex integer vector, in this case (51) cannot be satisfied. On the other hand, if $\alpha \neq 0$, based on the expression of $\mathbf{A}$ in (47), $\mathbf{A}$ is a full matrix with each element in the non-diagonal equal to

$$\mathbf{A}\left(i,j\right) = \mathbf{Z}_m\left(i,j\right), \ \forall i \neq j. \tag{52}$$

As $\mathbf{E}_l$ is a diagonal matrix, therefore it is observed that the right-hand side of (51) cannot be a diagonal matrix, which completes the proof. ■

Based on the Proposition 1, when employing quantized loads at the AP, there will always exist a performance loss compared to conventional MIMO even after the optimization. We then propose to minimize this performance gap by minimizing $\left\|\Delta\mathbf{i}\right\|^2$, where the following proposition is given.

Proposition 2: When the optimality for the optimization problem $\mathcal{P}_0$ is achieved, $\mathbf{t}^* = 0$, which means that any further changes in the quantized loads will result in an additional performance degradation.

Proof: When there is only a variation in the feeding voltage, we have an arbitrary $\alpha \neq 0$ and $\mathbf{t} = \mathbf{0}$. Then, based on (42) $\tilde{\mathbf{i}}$ can be expressed as

$$\begin{aligned}\tilde{\mathbf{i}} &= \left[diag\left(\tilde{\mathbf{z}}_L\right) + \mathbf{Z}_m\right]^{-1}\left(\mathbf{v}_s + \Delta\mathbf{v}\right) \\ &= \left(1+\alpha\right)\left\{\mathbf{i} - \left[diag\left(\tilde{\mathbf{z}}_L\right) + \mathbf{Z}_m\right]^{-1}\mathbf{E}_l\mathbf{i}\right\}.\end{aligned} \tag{53}$$

Then, for the same value of α, when a variation in the quantized loads is further introduced, $\mathbf{t} \neq \mathbf{0}$, based on (45) we have

$$\begin{aligned}\tilde{\mathbf{i}} = (1+\alpha)\Big\{&\mathbf{i} - [diag(\tilde{\mathbf{z}}_L) + \mathbf{Z}_m]^{-1}\mathbf{E}_l\mathbf{i} \\ &-[diag(\tilde{\mathbf{z}}_L) + \mathbf{Z}_m]^{-1} D \cdot diag(\mathbf{t})\,\mathbf{i}\Big\}.\end{aligned} \tag{54}$$

Comparing (54) with (53), it is clearly observed that an additional noise term is introduced in (54) due to the variation in the quantized loads, which then contributes to the increase in the power of the equivalent noise. Therefore, to keep the noise power as small as possible, the optimal case is to keep the quantized loads unchanged and optimize the feeding voltage only. ■

A. Closed-Form Solution

We then obtain the closed-form solution of the optimal α that minimizes $\|\Delta\mathbf{i}\|^2$. Based on the above proposition, the optimization problem is reduced to optimizing α only, which can be formulated as

$$\mathcal{P}_1: \ \min_{\alpha} \ \|\Delta\mathbf{i}\|^2 \tag{55}$$

Compared to $\mathcal{P}_0$, the constraint is also removed as we have $\mathbf{t}^* = \mathbf{0}$. Note that here $\mathbf{A}$, $\mathbf{E}_l$ and $\mathbf{i}$ are all known to the AP and α is the only variable to be optimized. In this case, $\Delta\mathbf{i}$ can be further expressed based on (48) as

$$\begin{aligned}\Delta\mathbf{i} &= (1+\alpha)\,\mathbf{A}^{-1}(\mathbf{A}-\mathbf{E}_l)\,\mathbf{i} - \mathbf{i} \\ &= \left(\mathbf{I} - \mathbf{A}^{-1}\mathbf{E}_l\right)\mathbf{i}\cdot\alpha + \left[\left(\mathbf{I} - \mathbf{A}^{-1}\mathbf{E}_l\right) - \mathbf{I}\right]\mathbf{i} \\ &= \mathbf{P}\cdot\alpha + (\mathbf{P} - \mathbf{i}),\end{aligned} \tag{56}$$

where we denote $\mathbf{P} = \left(\mathbf{I} - \mathbf{A}^{-1}\mathbf{E}_l\right)\mathbf{i}$ and $\mathbf{P} \in \mathcal{C}^{N_t \times 1}$. Then, we can further express $\|\Delta\mathbf{i}\|^2$ as

$$\begin{aligned}&\|\Delta\mathbf{i}\|^2 \\ &= tr\left\{\Delta\mathbf{i}\cdot\Delta\mathbf{i}^H\right\} \\ &= tr\left\{[\mathbf{P}\cdot\alpha + (\mathbf{P}-\mathbf{i})]\,[\mathbf{P}\cdot\alpha + (\mathbf{P}-\mathbf{i})]^H\right\} \\ &= tr\left\{\mathbf{P}\alpha\alpha^H\mathbf{P}^H\right\} + tr\left\{\left(\mathbf{P}\mathbf{P}^H - \mathbf{P}\mathbf{i}^H\right)\alpha\right\} \\ &+ tr\left\{\left[\left(\mathbf{P}\mathbf{P}^H - \mathbf{P}\mathbf{i}^H\right)\alpha\right]^H\right\} + tr\left\{(\mathbf{P}-\mathbf{i})(\mathbf{P}-\mathbf{i})^H\right\} \\ &= tr\left\{\mathbf{P}^H\mathbf{P}\alpha\alpha^H\right\} + 2\Re\left\{tr\left[\left(\mathbf{P}\mathbf{P}^H - \mathbf{P}\mathbf{i}^H\right)\alpha\right]\right\} \\ &+ tr\left\{(\mathbf{P}-\mathbf{i})(\mathbf{P}-\mathbf{i})^H\right\}.\end{aligned} \tag{57}$$

As $\mathbf{P}$ and $\mathbf{i}$ are independent of the variable α, the optimization problem can be transformed into

$$\mathcal{P}_2: \ \min_{\alpha} \ \ f(\alpha) \tag{58}$$

where

$$\begin{aligned}f(\alpha) &= tr\left\{\mathbf{P}^H\mathbf{P}\alpha\alpha^H\right\} + 2\Re\left\{tr\left[\left(\mathbf{P}\mathbf{P}^H - \mathbf{P}\mathbf{i}^H\right)\alpha\right]\right\} \\ &= tr\left\{S\cdot\alpha\alpha^H\right\} + 2\Re\left[tr\left(\mathbf{T}\cdot\alpha\right)\right].\end{aligned} \tag{59}$$

In (59), S and $\mathbf{T}$ are obtained as

$$S = \mathbf{P}^H\mathbf{P} > 0, \ \ \mathbf{T} = \mathbf{P}\mathbf{P}^H - \mathbf{P}\mathbf{i}^H. \tag{60}$$

By denoting

$$\Re(\alpha) = \alpha_{RE}, \ \ \Im(\alpha) = \alpha_{IM}, \tag{61}$$

the objective function in (59) can be further obtained as

$$\begin{aligned}f(\alpha) &= S\cdot\left(\alpha_{RE}^2 + \alpha_{IM}^2\right) + 2\sum_{i=1}^{N_t}\Re\left[\mathbf{T}(i,i)\right]\alpha_{RE} \\ &- 2\sum_{i=1}^{N_t}\Im\left[\mathbf{T}(i,i)\right]\alpha_{IM} \\ &= \left\{S\alpha_{RE}^2 + 2\sum_{i=1}^{N_t}\Re\left[\mathbf{T}(i,i)\right]\alpha_{RE}\right\} \\ &+ \left\{S\alpha_{IM}^2 - 2\sum_{i=1}^{N_t}\Im\left[\mathbf{T}(i,i)\right]\alpha_{IM}\right\}\end{aligned} \tag{62}$$

It is observed from (62) that $f(\alpha)$ is in a quadratic form for both the real part and the imaginary part of α, based on which we can then obtain the optimal α as

$$\alpha^* = \frac{-\sum_{i=1}^{N_t}\Re\left[\mathbf{T}(i,i)\right]}{S} + j\cdot\frac{\sum_{i=1}^{N_t}\Im\left[\mathbf{T}(i,i)\right]}{S}, \tag{63}$$

where j denotes the imaginary unit. With (63), the optimal feeding voltage can be efficiently obtained as

$$\tilde{\mathbf{v}}_s^* = (1+\alpha^*)\,\mathbf{v}_s. \tag{64}$$

With the closed-form solution obtained, the proposed scheme can be efficiently applied without significant complexity burden.

VI. Practical Implementation Aspects

It is observed that ESPAR-based MIMO systems require the adaption of each load impedance z_k dependent on the transmit symbols. It has been shown in [44] and the references therein that vactor technologies that can support the adaptive tuning have been developed and can be divided into three categories: semiconductor-based varactor diodes, micro-electro-mechanical system (MEMS) varactors, and ferroelectric-based varactors. Among them, semiconductor-based and ferroelectric-based varactors can support the tuning speed as fast as 100ns-100μs [44]-[46]. Such techniques can then be applied to ESPAR-based MIMO systems to support the adaptive impedance tuning. A proof-of-concept experiment has been conducted in [22], which supports the implementation of the ESPAR-based MIMO systems.

On the other hand, the adaptive impedance tuning on each antenna element may lead to variations on the input impedance of the ESPAR array, which will have an impact on the power transfer efficiency. For maximum power transfer, the impedance of the source should be equal to the conjugate of the input impedance of the ESPAR array to minimize any mismatch effects. Such a dynamic matching network can be implemented with lumped elements and varactor diodes [24][26].

VII. Energy Efficiency

To evaluate the usefulness of the ESPAR-based MIMO system in practice, we will investigate the tradeoff between the performance and the power consumption by means of the resulting energy efficiency. In this section,we define the energy efficiency of the communication system as the average achievable sum rate per total transmit power consumed, shown as [6][8]

$$EE = \frac{R}{N_{RF} \cdot P_{AC} + P_0 + P_{PA}}, \tag{65}$$

where R is the achievable sum rate, P_{AC} is the constant radio frequency (RF) circuit power consumption per antenna element, P_0 is the fixed power consumption that corresponds to the baseband processing for the antenna array, $P_{PA} = (1/\varepsilon - 1)P/e_{ant}$ denotes the total power consumption for the power amplifier where ε is the power amplifier efficiency [5]. e_{ant} is the radiation efficiency of the antenna and is defined as [47][48]

$$e_{ant} = e_{RL} e_{rad}, \tag{66}$$

where $e_{RL} = 1 - |\rho|^2$ is the efficiency caused by reflection effect, and the reflection coefficient ρ is obtained as $\rho = \frac{Z_{in} - z_0}{Z_{in} + z_0}$, which is based on the input impedance. $e_{rad} = 1 - \frac{z_0 \cdot \sum_{m=2}^{N_t} |i_m|^2}{\mathrm{Re}\{z_{in}\} \cdot |i_1|^2}$ is the radiation efficiency caused by the dissipation of the antenna, which is defined as the ratio of the radiated power of the antenna to the power accepted by the antenna. Throughout the simulations, the values of each parameter are as follows: $\varepsilon = 0.35$, $P_{AC} = 33dBm$, and $P_0 = 40dBm$. It is worth noting that $N_{RF} = N_t$ for conventional MIMO and $N_{RF} = 1$ for the single-fed ESPAR implementation.

VIII. Numerical Results

To evaluate the performance of ESPAR-based MIMO systems, in this section numerical results based on Monte Carlo simulations are presented. QPSK modulation is employed to evaluate the BER performance. The simulation parameters in this section follow Table I in Section IV. B, and these parameters remain the same throughout the following simulations unless otherwise stated. We consider a total number of $K = 3$ users in the system. Averaged antenna radiation efficiency is applied in the simulations to explicitly show the relationship between the energy efficiency and the selected parameters. We also assume that MIMO CI has the same antenna efficiency as ESPAR CI to highlight the energy efficiency gain introduced by the reduced number of RF chains. While we employ CI precoding throughout the simulations, the proposed schemes apply to any other precoding or beamforming techniques.

Fig. 4 presents the BER performance of the proposed scheme under both perfect CSI and imperfect CSI with respect to the transmit SNR. When ideal continuous loads are assumed, ESPARs can radiate exactly the same as conventional MIMO, thus achieving a similar performance. The presence of the quantized loads leads to a mismatch effect and greatly degrades the system performance. With the optimized feeding

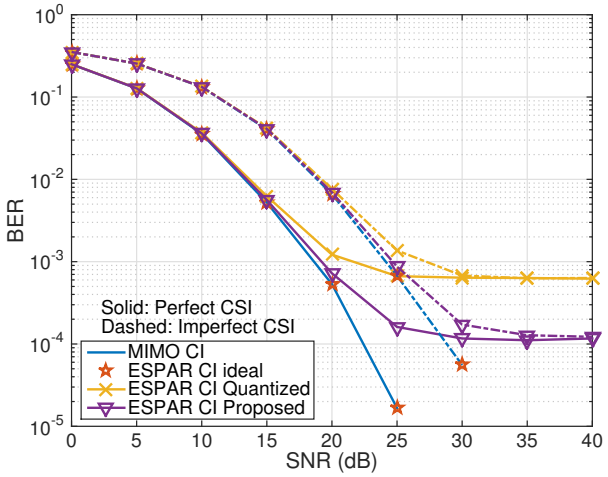

Fig. 4: BER comparison, $N_t = 5$, $K = 3$, quantization level $D = 1$, $\beta = 2.5$, QPSK

voltage obtained by the proposed scheme, the performance of ESPAR arrays with quantized loads are significantly improved, both for perfect CSI and imperfect CSI. The proposed scheme therefore enables the implementation of ESPAR arrays in practice. Note that the corresponding curves for perfect and imperfect CSI converge to the same error floor, which signifies that the quantization errors become dominant at high SNR.

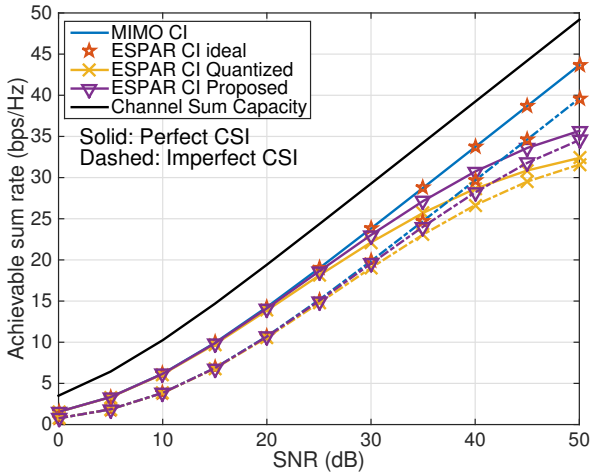

Fig. 5: Achievable sum rate, $N_t = 5$, $K = 3$, quantization level $D = 1$, $\beta = 2.5$

Fig. 5 compares the achievable sum rate of the proposed scheme of conventional MIMO and ESPAR with quantized loads with respect to the transmit SNR for both perfect CSI and imperfect CSI. The channel sum capacity is given by

$$C = \mathrm{E}\left\{ \sup_{\mathbf{G} \in \mathbf{A}} \log_2 \left[\det(\mathbf{I} + \frac{1}{\sigma^2} \mathbf{H}^H \mathbf{G} \mathbf{H}) \right] \right\} \tag{67}$$

where sup denotes the supremum function and $\mathbf{A}$ is the set of diagonal $K \times K$ matrices with nonnegative elements to ensure $tr(\mathbf{G}) = 1$. When equal transmit power allocation is assumed, $\mathbf{G} = (1/K) \cdot \mathbf{I}$. We note that, by the current vector

expression in (11), the typical Gaussian signaling assumption in the transmit symbols $\mathbf{s}$ translates directly to the antenna current vectors $\mathbf{i}$ in the ESPAR signal model. Accordingly, the Shannon formula above assuming Gaussian signals can still be applied to quantify the ESPAR performance. Then, it can be observed from Fig. 5 that with ideal load impedances, the ESPAR-based MIMO system can achieve the same rate performance as conventional MIMO. However in the presence of impedance errors by quantization, ESPARs are outperformed by conventional MIMO transmission. The proposed scheme is observed to achieve an improved performance compared to ESPAR with quantized loads and can better approach the performance of conventional MIMO, for both perfect CSI and imperfect CSI.

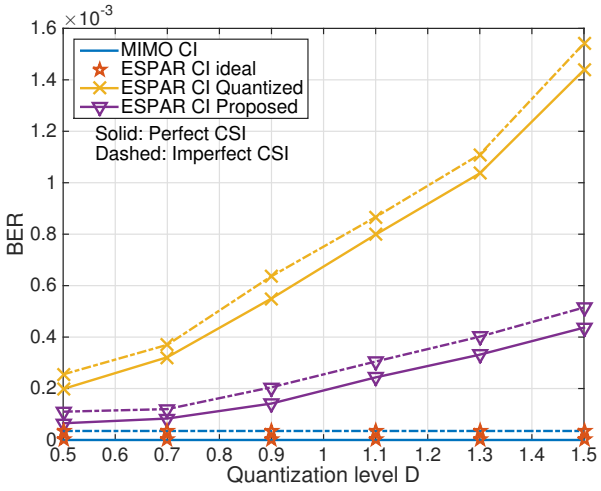

Fig. 6: BER comparison with respect to quantization level D, $N_t = 5$, $K = 3$, SNR=30dB, $\beta = 2.5$, QPSK

Fig. 6 compares the BER performance of conventional MIMO and ESPARs with an increasing quantization level D at the SNR of 30dB, under both perfect CSI and imperfect CSI. For conventional MIMO, the BER performance remains the same as impedance errors will not impact its performance. For ESPAR with quantized loads, as can be seen, the BER performance is degraded severely with the increase in the quantization level. For the proposed scheme, it can be observed that an improved performance can be achieved for both perfect CSI and imperfect CSI, where the impedance mismatch effect is greatly alleviated. It is also observed that the performance gains of the proposed scheme over ESPARs with quantized loads become more significant with the increase in the quantization level.

Fig. 7 shows the achievable sum rate of conventional MIMO and ESPARs with respect to the quantization level D under both perfect CSI and imperfect CSI. With an increase in the quantization level D, the performance gap between conventional MIMO and ESPARs with quantized loads becomes larger, as the impedance mismatch effect becomes more severe. For the proposed scheme, it is observed that it can better approach the rate performance of conventional MIMO for both perfect CSI and imperfect CSI. Furthermore, it is shown that the performance gains over ESPAR with quantized loads are

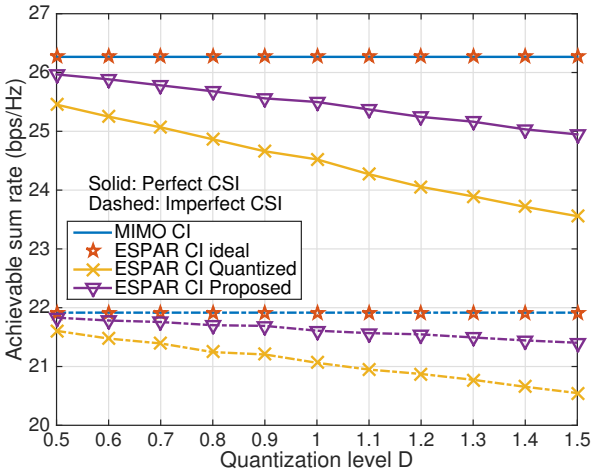

Fig. 7: Achievable sum rate with respect to quantization level D, $N_t = 5$, $K = 3$, SNR=30dB, $\beta = 2.5$

more significant with a larger value of the quantization level, which reveals the robustness of the proposed scheme even when quantization level is high.

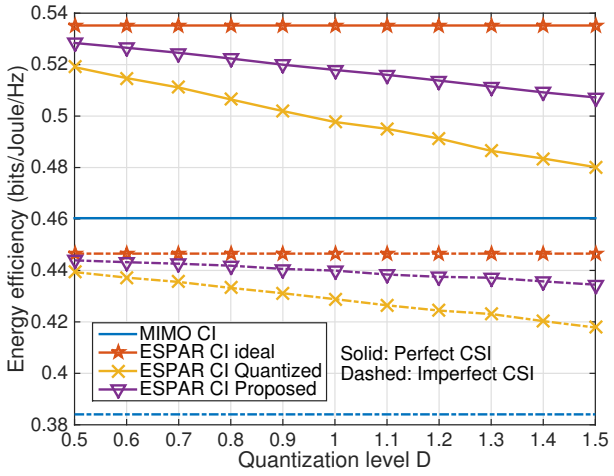

Fig. 8: Energy efficiency with respect to the quantization level D, $N_t = 5$, $K = 3$, SNR=30dB, $\beta = 2.5$

Fig. 8 shows the energy efficiency of conventional MIMO and ESPARs with respect to the quantization level D. For both perfect CSI and imperfect CSI, it is observed that almost all schemes based on ESPARs achieve a higher energy efficiency performance compared to conventional MIMO, which is due to the reduced number of RF chains required and the resulting reduced power consumption. Moreover, it is observed that in the presence of quantized loads, there will be an energy efficiency loss caused by the reduced sum rate performance, as shown in Fig. 7. For the proposed scheme, it can be seen that while there is still a slight performance degradation with the increase in the quantization level, it can better approach the energy efficiency performance of ESPARs with ideal continuous loads, for both perfect CSI and imperfect CSI.

Therefore, ESPARs with the proposed scheme can meet the requirement for the future green communications.

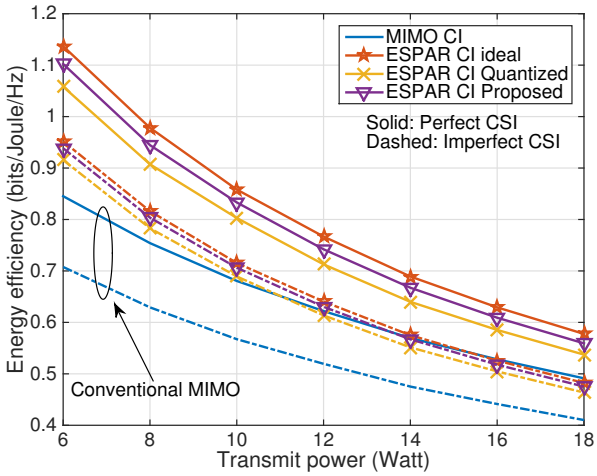

Fig. 9: Energy efficiency with respect to the transmit power, $N_t = 5$, $K = 3$, quantization level $D = 1$, SNR=30dB, $\beta = 2.5$

Fig. 9 compares the energy efficiency of conventional MIMO and ESPARs with the increase in the transmit power at SNR=30dB. For all schemes, the energy efficiency performance is reduced with the increase in the transmit power, as shown in (65). Moreover, it is observed that ESPAR systems with ideal continuous loads offers the highest energy efficiency due to the superior rate performance and the low power consumption. For the proposed optimization based scheme, it is observed that it improves the energy efficiency performance of ESPARs with quantized loads due to the superior rate performance, as shown in Fig. 5. For the imperfect CSI case, a similar performance trend can be observed, and the proposed scheme can approach the performance of ESPARs with the ideal continuous loads.

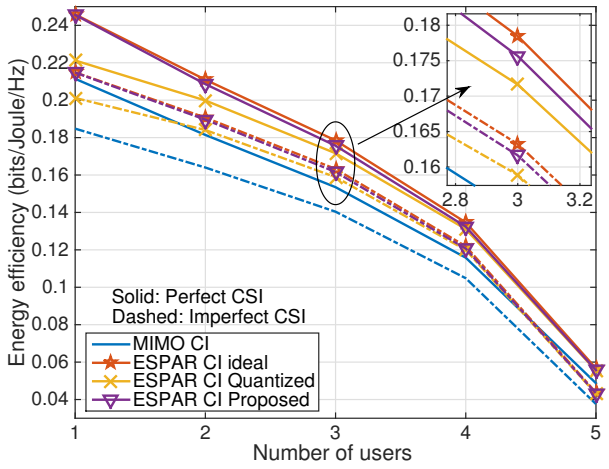

Fig. 10: Energy efficiency per user with respect to the number of users, $N_t = 5$, quantization level $D = 1$, SNR=30dB, $\beta = 2.5$

Fig. 10 shows the average energy efficiency per user for both conventional MIMO and ESPARs, where the transmit power is equally allocated to each user. With the increase in the number of users, the energy efficiency per user is reduced due to the reduced transmit power per user and the resulting reduced rate per user. Moreover, it is observed that conventional MIMO achieves the lowest energy efficiency performance due to the overwhelming power consumption for multiple RF chains. With the proposed scheme, ESPARs with quantized loads can achieve a similar energy efficiency performance to the ideal ESPAR arrays.

IX. Conclusion

In this paper the precoding techniques for ESPAR-based MIMO systems are studied. The exact computation of the tunable loads and feeding voltage is firstly obtained. Then, we analytically derive the received SNR and probability of error for CI precoding in the presence of quantized loads and imperfect CSI. It is shown that impedance errors introduced by quantization introduce an additional noise term. Furthermore, to compensate for the performance degradation, we propose a robust scheme where the optimal feeding voltage is obtained with a closed-form solution. Simulation results show that ESPARs with the ideal continuous loads can achieve a similar performance to conventional MIMO, while the proposed scheme can compensate for the performance loss introduced by the quantized loads. It is also shown that the energy efficiency results are more favourable for ESPAR based systems as only one RF chain is employed.

References

[1] *Evolved Universal Terrestrial Radio Access (E-UTRA); Physical channels and modulation*, 3GPP TS 36.211 V11.5.0, Release 11, 2013-12.

[2] *Evolved Universal Terrestrial Radio Access (E-UTRA); LTE physical layer; General description*, 3GPP TS 36.201 V10.0.0, Release 10, 2010-12.

[3] M. Costa, "Writing on Dirty Paper," *IEEE Trans. Inf. Theory*, vol. IT-29, no. 3, pp. 439–441, May 1983.

[4] M. B. Shenouda and T. N. Davidson, "A Framework for Designing MIMO Systems with Decision Feedback Equalization or Tomlinson-Harashima Precoding," *IEEE J. Sel. Areas Commun.*, vol. 26, no. 2, pp. 401–411, Feb. 2008.

[5] F.-S. Tseng, M.-Y. Chang, and W.-R. Wu, "Joint Tomlinson-Harashima Source and Linear Relay Precoder Design in Amplify-and-Forward MIMO Relay Systems via MMSE Criterion," *IEEE Trans. Veh. Tech.*, vol. 60, no. 4, pp. 1687–1698, March 2011.

[6] A. Li and C. Masouros, "A Two-Stage Vector Perturbation Scheme for Adaptive Modulation in Downlink MU-MIMO," *IEEE Trans. Veh. Tech.*, vol. 65, no. 9, pp. 7785–7791, Oct. 2015.

[7] B. M. Hochwald, C. B. Peel, and A. L. Swindlehurst, "A Vector-Perturbation Technique for Near-Capacity Multiantenna Multiuser Communication-part II: Perturbation," *IEEE Trans. Commun.*, vol. 53, no. 3, pp. 537–544, March 2005.

[8] A. Li and C. Masouros, "A Constellation Scaling Approach to Vector Perturbation for Adaptive Modulation in MU-MIMO," *IEEE Wireless Commun. Lett.*, vol. 4, no. 3, pp. 289–292, March 2015.

[9] C. Windpassinger, R. Fischer, T. Vencel, and J. Huber, "Precoding in Multiantenna and Multiuser Communications," *IEEE Trans. Wireless Commun.*, vol. 3, no. 4, pp. 1305–1316, July 2004.

[10] M.-C. Lee, W.-H. Chung, and T.-S. Lee, "Generalized Precoder Design Formulation and Iterative Algorithm for Spatial Modulation in MIMO Systems with CSIT," *IEEE Trans. Commun.*, vol. 63, no. 4, pp. 1230–1244, April 2015.

[11] T. Haustein, C. von Helmolt, E. Jorswieck, V. Jungnickel, and V. Pohl, "Performance of MIMO Systems with Channel Inversion," in *Proc. 55th IEEE Veh. Tech. Conf. (VTC)*, vol. 1, Birmingham, AL, May 2002, pp. 35–39.

[12] C. B. Peel, B. M. Hochwald, and A. L. Swindlehurst, "A Vector-Perturbation Technique for Near-Capacity Multiantenna Multiuser Communication-part I: Channel Inversion and Regularization," *IEEE Trans. Commun.*, vol. 53, no. 1, pp. 195–202, Jan. 2005.

[13] C. Masouros, "Correlation Rotation Linear Precoding for MIMO Broadcast Communications," *IEEE Trans. Sig. Process.*, vol. 59, no. 1, pp. 252–262, Jan. 2011.

[14] K. Gyoda and T. Ohira, "Design of Electronically Steerable Passive Array Radiator (ESPAR) Antennas," in *IEEE Antennas and Propagation Society International Symposium. Transmitting Waves of Progress to the Next Millennium. 2000 Digest. Held in conjunction with: USNC/URSI National Radio Science Meeting*, vol. 2, Salt Lake City, UT, USA, 2000, pp. 922–925.

[15] M. D. Migliore, "An Intuitive Electromagnetic Approach to MIMO Communication Systems," *IEEE Ant. and Propag. Mag.*, vol. 48, no. 3, pp. 128–137, June 2006.

[16] A. Kalis, A. G. Kanatas, and C. B. Papadias, "A Novel Approach to MIMO Transmission Using a Single RF Front End," *IEEE J. Sel. Areas Commun.*, vol. 26, no. 6, pp. 972–980, Aug. 2008.

[17] O. N. Alrabadi, C. B. Papadias, A. Kalis, and R. Prasad, "A Universal Encoding Scheme for MIMO Transmission Using a Single Active Element for PSK Modulation Schemes," *IEEE Trans. Wireless Commun.*, vol. 8, no. 10, pp. 5133–5143, Oct. 2009.

[18] P. N. Vasileiou, K. Maliatsos, E. D. Thomatos, and A. G. Kanatas, "Reconfigurable Orthonormal Basis Patterns Using ESPAR Antennas," *IEEE Ant. and Wireless Propag. Lett.*, vol. 12, pp. 448–451, March 2013.

[19] Y. Zhou, R. S. Adve, and S. V. Hum, "Design and Evaluation of Pattern Reconfigurable Antennas for MIMO Applications," *IEEE Trans. Ant. and Propag.*, vol. 62, no. 3, pp. 1084–1092, Oct. 2013.

[20] A. Kalis, A. G. Kanatas, and C. B. Papadias, *Parasitic Antenna Arrays for Wireless MIMO Systems*. New York: Springer, 2014.

[21] B. Han, V. I. Barousis, A. Kalis, C. B. Papadias, A. G. Kanatas, and R. Prasad, "A single RF MIMO Loading Network for High Order Modulation Schemes," *Int. J. of Ant. and Propag.*, vol. 3, pp. 1–10, 2014.

[22] O. N. Alrabadi, C. Divarathne, P. Tragas, A. Kalis, N. Marchetti, C. B. Papadias, and R. Prasad, "Spatial Multiplexing with a Single Radio: Proof-of-Concept Experiments in an Indoor Environment with a 2.6GHz Prototype," *IEEE Wireless Commun. Lett.*, vol. 15, no. 2, pp. 178–180, Feb. 2011.

[23] B. Han, V. I. Barousis, C. B. Papadias, A. Kalis, and R. Prasad, "MIMO over ESPAR with 16-QAM Modulation," *IEEE Wireless Commun. Lett.*, vol. 2, no. 6, pp. 687–690, Dec. 2013.

[24] V. I. Barousis and C. B. Papadias, "Arbitrary Precoding with Single-Fed Parasitic Arrays: Closed-Form Expression and Design Guidelines," *IEEE Wireless Commun. Lett.*, vol. 3, no. 2, pp. 229–232, April 2014.

[25] V. I. Barousis, R. R. Muller, and C. B. Papadias, "A New Signal Model for MIMO Communication with Compact Parasitic Arrays," in *2014 6th International Symposium on Communications, Control and Signal Processing (ISCCP)*, Athens, 2014, pp. 109–113.

[26] L. Zhou, F. A. Khan, T. Ratnarajah, and C. B. Papadias, "Achieving Arbitrary Signals Transmission Using a Single Radio Frequency Chain," *IEEE Trans. Commun.*, vol. 63, no. 12, pp. 4865–4878, Oct. 2015.

[27] M. A. Sedaghat, V. I. Barousis, R. R. Muller, and C. B. Papadias, "Load Modulated Arrays: a Low-Complexity Antenna," *IEEE Commun. Mag.*, vol. 54, no. 3, pp. 26–52, March 2016.

[28] A. Li and C. Masouros, "Performance Analysis for Single-Fed ESPAR in the Presence of Imepdance Errors and Imperfect CSI," in *2016 IEEE International Conference on Communications (ICC)*, Kuala Lumpur, 2016, pp. 1–6.

[29] D. J. R. Chisaguano, Y. Hou, T. Higashino, and M. Okada, "Low Complexity Channel Estimation and Detection for MIMO-OFDM Receiver with ESPAR Antennas," *IEEE Trans. Veh. Tech.*, vol. 65, no. 10, pp. 8297–8308, Oct. 2016.

[30] D. J. R. Chisaguano and M. Okada, "MIMO-OFDM Receiver Using a Modified ESPAR Antenna with Periodically Changed Directivity," in *2013 13th International Symposium on Communications and Information Technologies (ISCIT)*, Surat Thani, 2013, pp. 154–159.

[31] G. C. Alexandropoulos, V. I. Barousis, and C. B. Papadias, "Precoding for Multiuser MIMO Systems with Single-Fed Parasitic Antenna Arrays," in *2014 IEEE Global Communications Conference*, Austin, TX, 2014, pp. 3897–3902.

[32] C. Wang and R. D. Murch, "Adaptive Downlink Multi-user MIMO Wireless Systems for Correlated Channels with Imperfect CSI," *IEEE Trans. Wireless Commun.*, vol. 5, no. 9, pp. 2435–2446, Sept. 2006.

[33] C. Masouros, M. Sellathurai, and T. Ratnarajah, "Large-Scale MIMO Transmission in Fixed Physical Spaces: the Effect of Transmit Correlation and Mutual Coupling," *IEEE Trans. Commun.*, vol. 61, no. 7, pp. 2794–2804, July 2013.

[34] D. S. Holder, Ed., *Electrical Impedance Tomography: Methods, History and Applications*. CRC Press, Dec. 2004.

[35] S. L. Carson, M. E. Orazem, O. D. Crisalle, and L. Garcia-Rubio, "On the Error Structure of Imepdance Measurements - Simulation of FRA Instrumentation," *Journal of the Electrochemical Society*, vol. 150, no. 10, pp. 477–490, 2003.

[36] ——, "On the Error Structure of Imepdance Measurements - Series Expansions," *Journal of the Electrochemical Society*, vol. 150, pp. 501–511, 2003.

[37] G. L. Stuber, *Principles of Mobile Communication*, 3rd ed. New York: Springer, Sept. 2011.

[38] J. Maurer, J. Jalden, D. Seethaler, and G. Matz, "Vector Perturbation Precoding Revisited," *IEEE Trans. Sig. Process.*, vol. 59, no. 1, pp. 315–328, Jan. 2011.

[39] D. Gore, R. W. Heath, and A. Paulraj, "On Performance of the Zero Forcing Receiver in Presence of Transmit Correlation," in *Proceedings IEEE International Symposium on Information Theory*, 2002, pp. 159–.

[40] R. Xu and F. C. M. Lau, "Performance Analysis for MIMO Systems Using Zero Forcing Dector over Fading Channels," *Communications, IEE Proceedings*, vol. 153, no. 1, pp. 74–80, Feb. 2006.

[41] M. Kiessling and J. Speidel, "Analytical Performance of MIMO Zero-Forcing Receivers in Correlated Rayleigh Fading Environments," in *4th IEEE Workshops on Signal Processing Advances in Wireless Communications (SPAWC)*, 2003, pp. 383–387.

[42] C. A. Balanis, *Antenna Theory: Analysis and Design*, 3rd ed. John Wiley and Sons, 2005.

[43] Q. Zhang, C. He, and L. Jiang, "Per-Stream MSE based Linear Transceiver Design for MIMO Interference Channels with CSI Error," *IEEE Trans. Commun.*, vol. 63, no. 5, pp. 1676–1689, May 2015.

[44] J.-S. Fu, "Adaptive Impedance Matching Circuits based on Ferroelectric and Semiconductor Varactors," *Ph. D. dissertation*, University of Michigan 2009.

[45] R. York, A. Nagra, E. Erker, T. Taylor, P. Periaswamy, J. Speck, S. Streiffer, and O. Auciello, "Microwave Integrated Circuits Using Thin-film BST," in *Proceedings of the 2000 12th IEEE International Symposium on Applications of Ferroelectrics (ISAF 2000)*, vol. 1, Honolulu, HI, 2000, pp. 195–200.

[46] J.-S. Fu, X. A. Zhu, J. D. Phillips, and A. Mortazawi, "Improving Linearity of Ferroelectric-based Microwave Tunable Circuits," *IEEE Trans. Microwave Theory and Techniques*, vol. 55, no. 2, pp. 354–360, Feb. 2007.

[47] R. Prabhu and B. Daneshrad, "Energy-Efficient Power Loading for a MIMO-SVD System and Its Performance in Flat Fading," in *2010 IEEE Global Telecommunications Conference (GLOBECOM 2010)*, Miami, FL, 2010, pp. 1–5.

[48] P. Kildal and K. Rosengren, "Electromagnetic Analysis of Effective and Apparent Diversity Gain of Two Parallel Dipoles," *IEEE Ant. and Wireless Propag. Lett.*, vol. 2, no. 1, pp. 9–13, Feb. 2003.

Ang Li (S'14) received the Bachelor and Master degree in Electronic and Information Engineering from Xi'an Jiaotong University in 2011 and 2014, respectively. He is currently pursuing his Ph.D. degree in the Communications and Information Systems research group, Dept. Electrical & Electronic Engineering, University College London. His research interests lie in the field of wireless communications with focus on beamforming designs for MIMO systems and ESPAR-based systems.

Christos Masouros (M'06-SM'14) received the Diploma degree in Electrical and Computer Engineering from the University of Patras, Greece, in 2004, and MSc by research and PhD in Electrical and Electronic Engineering from the University of Manchester, UK in 2006 and 2009 respectively. In 2008 he was a research intern at Philips Research Labs, UK. Between 2009-2010 he was a Research Associate in the University of Manchester and between 2010-2012 a Research Fellow in Queen's University Belfast. He has held a Royal Academy of Engineering Research Fellowship between 2011-2016.

He is currently a Senior Lecturer in the Communications and Information Systems research group, Dept. Electrical & Electronic Engineering, University College London. His research interests lie in the field of wireless communications and signal processing with particular focus on Green Communications, Large Scale Antenna Systems, Cognitive Radio, interference mitigation techniques for MIMO and multicarrier communications. He was the recipient of the Best Paper Award in the IEEE GlobeCom conference 2015, and has been recognised as an Exemplary Editor for the IEEE Communications Letters, and as an Exemplary Reviewer for the IEEE Transactions on Communications. He is an Associate Editor for IEEE Communications Letters, and Guest Editor for IEEE Journal on Selected Topics in Signal Processing issue "Exploiting Interference towards Energy Efficient and Secure Wireless Communications".

Constantinos B. Papadias is the Dean of Athens Information Technology (AIT), in Athens, Greece, where he is also a Professor and Head of its Broadband Wireless and Sensor Networks (B-WiSE) Research Group. He is also an Adjunct Professor at Alaborg University in Denmark. He received the Diploma of Electrical Engineering from the National Technical University of Athens (NTUA) in 1991 and the Doctorate degree in signal processing (highest honors) from the Ecole National Suprieure des Telecommunications (ENST), Paris, France, in 1995. He was a researcher at Institut Eurecom (1992-1995), Stanford University (1995-1997) and Bell Labs (as a member of technical staff from 1997-2001 and as a technical manager from 2001-2006). He was also an Adjunct Professor at Columbia University (2004-2005) and Carnegie Mellon University (2006-2011). His research interests span several areas of advanced communication systems, with emphasis on wireless, cognitive, green and next generation networks. He has published over 170 papers, one research monograph, two edited books, 5 book chapters, and has received over 6000 citations for his work. He has also made standards contributions and held 12 patents. He was a member of the Steering Board of the Wireless World Research Forum (WWRF) from 2002-2006, a member and industrial liaison of the IEEE's Signal Processing of Communications Technical Committee from 2003-2008 and a National Representative of Greece to the European Research Council's IDEAS program from 2007-2008. He has served as a member of the IEEE Communications Society's Fellow Evaluation and Awards Comities, as well as an Associate Editor for the IEEE Transactions on Signal Processing, the IEEE Transactions on Wireless Communications and the Journal of Communications and Networks. He has participated in several European Commission research grants, including the recently awarded (Horizon2020) project SANSA in the area of satellite-assisted wireless backhauling and another two FP7 research projects where he acts as technical coordinator: HARP, in the area of remote radio heads, and ADEL, in the area of licensed shared access. His distinctions include the Bell Labs President's award (2002); a Bell Labs Teamwork Award (2003); the IEEE Signal Processing Society's Young Author Best Paper Award (2003); ESI's most cited paper of the decade citation in the area of wireless networks (2006); his recognition as a highly cited Greek scientist (2011); and the co-authorship of two papers that earned Best Student Paper Awards at the IEEE International Conference on Bioinformatics and BioEngineering (2013&2014). He was a Distinguished Lecturer of the IEEE Communications Society for 2012-2013. Dr. Papadias is a member of the Technical Chamber of Greece and a Fellow of IEEE.